


3D track reconstruction capability of a silicon hybrid active pixel detector

Benedikt Bergmann^{1,a} , Martin Pichotka¹, Stanislav Pospisil¹, Jiri Vycpalek¹, Petr Burian^{1,2}, Pavel Broulim^{1,2}, Jan Jakubek³

¹ Institute of Experimental and Applied Physics, Czech Technical University in Prague, Horská 22/3a, 128 00 Praha 2, Czech Republic

² Faculty of Electrical Engineering, University of West Bohemia, Univerzitní 26, Pilsen, Czech Republic

³ Advacam s.r.o., U Pergamenky 12, 170 00 Praha 7, Czech Republic

Received: 14 March 2017 / Accepted: 15 June 2017 / Published online: 23 June 2017

© The Author(s) 2017. This article is an open access publication

Abstract Timepix3 detectors are the latest generation of hybrid active pixel detectors of the Medipix/Timepix family. Such detectors consist of an active sensor layer which is connected to the readout ASIC (application specific integrated circuit), segmenting the detector into a square matrix of 256×256 pixels (pixel pitch $55 \mu\text{m}$). Particles interacting in the active sensor material create charge carriers, which drift towards the pixelated electrode, where they are collected. In each pixel, the time of the interaction (time resolution 1.56ns) and the amount of created charge carriers are measured. Such a device was employed in an experiment in a $120\text{GeV}/c$ pion beam. It is demonstrated, how the drift time information can be used for “4D” particle tracking, with the three spatial dimensions and the energy losses along the particle trajectory (dE/dx). Since the coordinates in the detector plane are given by the pixelation (x, y), the x - and y -resolution is determined by the pixel pitch ($55 \mu\text{m}$). A z -resolution of $50.4 \mu\text{m}$ could be achieved (for a $500 \mu\text{m}$ thick silicon sensor at 130V bias), whereby the drift time model independent z -resolution was found to be $28.5 \mu\text{m}$.

1 Introduction

The Timepix3 [1] is the latest development in the series of hybrid active pixel detectors of the Medipix/Timepix family, which – in contrast to its predecessors – allows a simultaneous measurement of the time and the energy in each pixel. Detectors of the Timepix [2] technology have been employed in various applications, which include life science (imaging, hadron therapy, ...) [3,4], the measurement of angular correlation functions [5], space weather analyses [6], the determi-

nation of trapped particle directions in the radiation belts [7], or the study of the antiproton annihilation [8]. In particular Timepix detectors with a CdTe or CdZnTe sensor layer have been considered for double beta decay experiments [9]. A majority of these applications would profit significantly from a determination of the interaction depth in the active sensor, e.g. by improving particle discrimination, background event suppression, annihilation vertex reconstruction, or impact angle determination.

Filipenko et al. [10] presented a method for a 3D track reconstruction and achieved a z -resolution of $60 \mu\text{m}$ utilizing a Timepix chip attached to a 1mm thick CdTe sensor. However, due to the limited time resolution of the Timepix chip, they had to use the sensor at very low bias, thus losing charge due to recombination. Additionally, they had to deal with the problem of not measuring directly the energy, which is needed for a proper time assignment. The Timepix3 readout chip’s improved time resolution and its capability of measuring the energy and time simultaneously in each pixel overcomes both issues. Turecek et al. [11] and Pacifico et al. [8] recently presented 3D reconstructions of particle trajectories with the Timepix3 readout chip attached to silicon sensors. It is the aim of the presented work to follow up on this by further improving and standardizing the methods for the z -reconstruction, and by presenting a detailed study of the achievable z -resolutions.

The article is structured as follows. The Timepix3 detector technology and its working principle are described in Sect. 2. In Sect. 3 a drift time model is derived and the time stamp correction is outlined. In Sect. 4, the presented drift time model is validated by data measured in a $120\text{GeV}/c$ pion beam and the z -resolution is determined. Before the results are discussed in Sect. 6, in Sect. 5 3D reconstructed pion ($120\text{GeV}/c$) and muon (from the natural background) events are illustrated.

^a e-mail: benedikt.bergmann@utef.cvut.cz

2 The Timepix3 detector

2.1 Basic facts

Timepix3 devices are state-of-the-art hybrid active pixel detectors, developed within the Medipix3 Collaboration as the successors of the Timepix. They consist of an active sensor layer, which is bump-bonded to the readout ASIC. The readout chip is designed in 130 nm CMOS technology and segments the active sensor layer into 256×256 pixels with a pixel-to-pixel distance (pixel pitch) of $55 \mu\text{m}$. It can be used in a data-driven readout scheme measuring simultaneously the time of an interaction with 1.56 ns resolution and the energy deposit in each pixel. The dead time per pixel is 475 ns for hit rates of up to $40 \text{ Mhits cm}^{-2}\text{s}^{-1}$. The Ethernet embedded readout interface for the Timepix3, the “Kathrine readout”¹, developed in the Institute of Experimental and Applied Physics in cooperation with the Faculty of Electrical Engineering of the University of West Bohemia (in Pilsen), was used for detector control.

2.2 Working principle

Upon the interaction of ionizing radiation in the sensor layer, electron hole pairs are created. Due to an applied electric field these charge carriers drift towards either of the electrodes. In the silicon sensor, used in this work, the holes drift towards the pixelated cathode, the electrons towards the common anode (a further discussion is given in Sect. 3). During drift and collection, the created charge carriers induce currents, which are converted into voltage pulses, in the pixel electrodes nearest to their current position. After the amplification and shaping, the voltage pulses are compared to a threshold level (THL), which is adjusted to a global value after a per-pixel threshold equalization. The threshold is needed to provide a noiseless operation in the presence of the electronic noise of the readout chip. The minimal threshold required depends on the characteristics of the particular chip. For the Timepix3 with proper cooling a minimal threshold of 1.8 keV could be achieved. However, for the presented experiment it was set conservatively to 3 keV . One inherent consequence of using a comparator with an adjustable, non-zero threshold for signal discrimination is the so-called time-walk effect, which is addressed in Sect. 3.2.

In Fig. 1 the processing in the analog part of the pixel electronics is illustrated. The preamplifier output signal is modeled by a triangular pulse (black line). As the pulse of the amplifier traverses the preset threshold, both, the energy

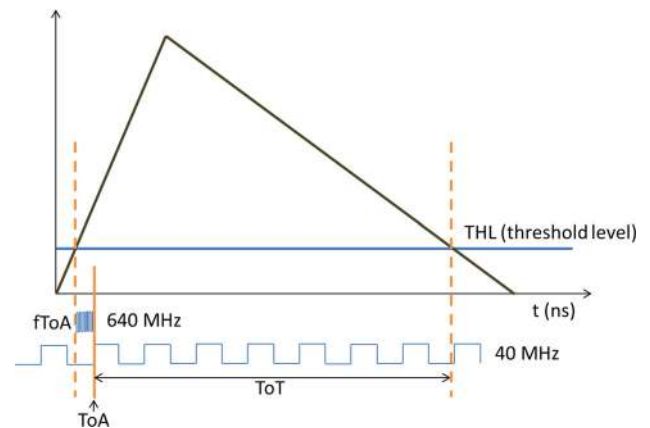


Fig. 1 Principle of the time and energy detection of a Timepix3 readout chip

(the so-called time-over-threshold, ToT) as well as the time-of-arrival (ToA) are initiated. In order to provide a highly accurate ToA information the current Timepix3 chip features a 640 MHz clock which is started upon the signal crossing the threshold in addition to the 40 MHz base clock. By this the time resolution of 1.56 ns is achieved. The ToT measurement on the other hand employs the base clock of 40 MHz to sample the time during which the signal stays above the threshold, resulting in an energy resolution comparable to the previous generation of the chip. The energy dependence of the ToT response can be calibrated using photons of known energy, e.g. x-ray fluorescence lines [12].

3 Reconstruction method

To obtain 3D information, the Timepix3 detector is used similarly to a time projection chamber (TPC) [13, 14]: The spatial coordinates in the x - and y -plane are given by the pixelation of the sensor layer, whereas the z -coordinate is reconstructed from the time the charge carriers (in our case holes) need to drift towards the pixel electrodes. This section outlines the track reconstruction procedure and the necessary time-walk correction.

The analysis presented here considers the relative change of the drift times along a particle track. Therefore, it should be noted, that currently absolute depth information cannot be obtained for particles, which do not penetrate the sensor layer completely, as this would require a reference time signal. A possible solution is discussed in Sect. 6.

3.1 Drift time model

Charge carriers created in the sensor material by an ionizing particle drift through the sensor material due to the applied voltage difference between the unpixelated back side con-

¹ The contribution “Katherine: Ethernet Embedded Readout Interface for Timepix3” was accepted for the 19th International Workshop on Radiation Imaging Detectors and will be published in the conference proceedings in the Journal of Instrumentation.

tact ($z = d$, d : thickness of the sensor) and the pixelated cathode ($z = 0$). The drift velocities of the charge carriers (electrons, holes) are determined by their mobilities μ_e, μ_h and the electric field according to

$$v_{e,h} = \mu_{e,h} E. \tag{1}$$

In a homogeneously doped sensor, the electric field as a function of sensor depth z can be described by:

$$E = \frac{U_B}{d} + \frac{2U_D}{d^2} \left(\frac{d}{2} - z \right) e_z \tag{2}$$

with the sensor thickness d , the depletion voltage U_D , and the bias voltage U_B [15]. Since a p-on-n (p+ contact on a high resistivity n+ bulk) silicon sensor was used, the measured signal is created by the positive charge carriers (i.e. holes). Inserting Eq. (2) into Eq. 1, we obtain the differential equation

$$v = \frac{\mu_h U_B}{d} e_z + \frac{2\mu_h U_D}{d^2} \left(\frac{d}{2} - z \right) e_z = \frac{dz}{dt} e_z, \tag{3}$$

which is solved by the ansatz

$$z(t) = \frac{d}{U_D} (U_D + U_B) \left[1 - \exp \left(\frac{2U_D \mu_h}{d^2} t \right) \right]. \tag{4}$$

Likewise, the z dependence of the drift time is

$$t(z) = -\frac{d^2}{2U_D \mu_h} \ln \left(1 - \frac{2U_D}{U_D + U_B} \frac{z}{d} \right). \tag{5}$$

3.2 Time-walk correction

Since the amplifier employed in the front-end electronics of the chip features a fixed signal rise time of less than 25 ns, whereas the signal height corresponds linearly to the charge deposited within the pixel, the rising signal of the preamplifier intersects the THL level at a different times for different pulse heights. As illustrated in Fig. 2, an event with a higher final signal height intersects the THL at an earlier time than a signal featuring a lower signal height. This behavior is known as time-walk effect.

To correct the measured time stamps for the time-walk, we used the experimental approach described in [11]. The detector was irradiated by 59.6 keV gamma-rays from an ^{241}Am -source. Upon interaction with the sensor material these photons create free charge carriers in a small volume. Thus, these interactions are mostly observed as single-pixel clusters. However, due to charge-sharing, photons hitting the pixelated sensor at the edges of pixels result in clusters with up to 4 pixels.

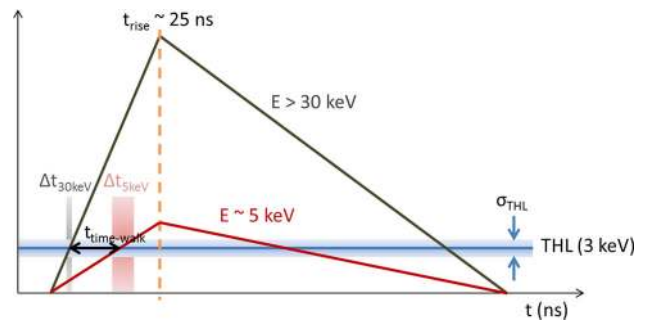


Fig. 2 Illustration of the time-walk effect: a low energy signal, occurring in the same time as a higher energy signal is assigned to a later time stamp

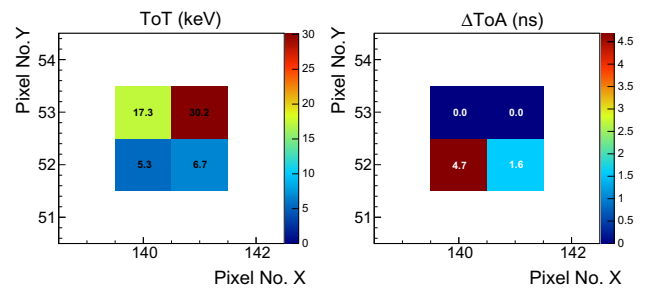


Fig. 3 Typical 4-pixel cluster as seen in a measurement with an ^{241}Am source (photon energy 59.6 keV)

For the time-walk correction, such 4-pixel clusters with one of the pixels measuring 30–32 keV, were selected. A typical 4-pixel cluster is shown in Fig. 3.

The pixel with the 30–32 keV measurement determines the reference time stamp t_{ref} , defining the rising edge’s slope of a high energy signal. For each of the 3 remaining pixels, the unwanted delay due to the time-walk $t_{i,time-walk}$ is obtained by subtracting the pixel’s time stamp from the reference time: $t_{i,time-walk} = t_i - t_{ref}$.

The energy dependence of $t_{i,time-walk}$ can be studied using the per pixel energy information E_i . Figure 4a shows the scatter plot of measured pixel energies E_i versus their time delays $t_{i,time-walk}$ for 803,950 events. The width of the time-delay distributions increases for energies close to the threshold. As illustrated in Fig. 2, this can be explained by the fact that fluctuations of the THL (σ_{THL}) have a bigger effect on the measurement of the THL crossing times for lower signal heights: $\Delta t(E_1) < \Delta t(E_2)$, for $E_1 < E_2$. To avoid unreliable depth reconstructions, the time stamps of pixels with energies below 4 keV were omitted for the z -determination.

To obtain the time-walk correction function, the medians of the time delay distributions for each energy channel are calculated (see Fig. 4b) and fitted by the function

$$t_{time-walk}(E) = \frac{a}{(E - b)^c} + d, \quad 4 \text{ keV} < E < 30 \text{ keV}. \tag{6}$$

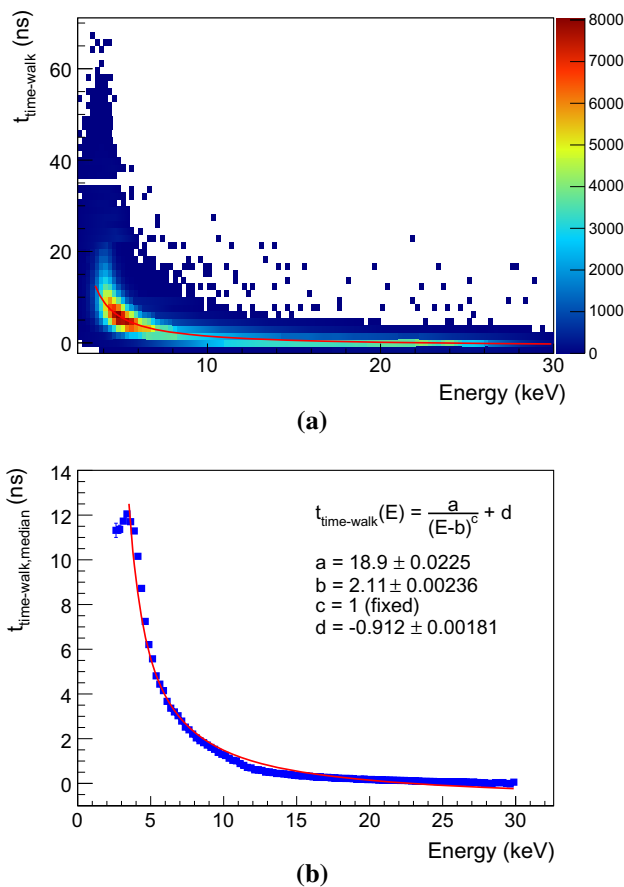


Fig. 4 **a** Scatter plot of delays due to the time-walk effect in dependence of the energy of pixels in a 4-pixel cluster with one pixel measuring 30–32 keV. The detector was irradiated by 59.6 keV gamma rays; **b** delay due to time-walk as a function of energy measured in the pixels. The subtraction of the value calculated for the pixel energy according to the fit curve corrects for the time-walk. Deviations of the data points from the fit are significantly smaller than the granularity of the time measurement (i.e. 1.56 ns). The fit is also indicated by the red line in **a**

With a fixed value $c = 1$, we find the parameters $a = (18.9 \pm 0.02)$ ns keV, $b = (2.11 \pm 0.002)$ keV, and $d = (-0.912 \pm 0.002)$ ns. The corrected time $t_{i,corr.}$ in each pixel was then given by:

$$t_{i,corr.} = t_i - \max(\{t_{time-walk}(E_i), 12.5 \text{ ns}\}). \tag{7}$$

4 Experimental results

An experiment to validate the drift time model and to determine the achievable z -resolutions was performed at the SPS (super proton synchrotron) at CERN. A Timepix3 with a 500 μm thick silicon sensor was irradiated by 120 GeV/c pions at the angles $\Theta = 60^\circ$ (angle to the sensor normal) and $\varphi = 0^\circ$ (angle to the x -axis). An illustrative set of 50 measured tracks is shown in Fig. 5.

For the following analyses, we define a prototypical event as a track containing 15 or 16 pixels, which is oriented parallelly to the x -axis, and select them by the criteria: $\Delta y = 0$ (maximal difference of row number) and $N_{\text{pixels}} \in [15; 16]$. Since, at the given angle of 60° a straight track of this length and orientation fully traverses the sensor in vertical direction, the z -coordinate $z_{i, \text{trajectory}}$ in each pixel i can be obtained geometrically when interpolating between the entry (sensor top) and exit point. Hereby, we have defined the entrance point as the rightmost pixel of the track (pixel with highest x value). For the exit point determination the pixel with the lowest measured time $x_{t_{\text{min}}}$ and its relative position within the track were of interested. Three cases were defined:

- Case 1: The pixel with the lowest measured time $x_{t_{\text{min}}}$ is the leftmost pixel x_{left} . In this case this pixel is defined as the exit point.
- Case 2: The pixel with the lowest measured time $x_{t_{\text{min}}}$ is next to the leftmost pixel x_{left} : $x_{\text{left}} = x_{t_{\text{min}}} - 1$. This typically happens when a particle leaves the sensor at the edge of a pixel. Some charge is then leaking into the neighboring pixel, which typically registers a higher time stamp. In this case the exit point was defined as the energy weighted average $x_{\text{exit}} = \frac{x_{t_{\text{min}}}E(x_{t_{\text{min}}}) + x_{\text{left}}E(x_{\text{left}})}{E(x_{t_{\text{min}}}) + E(x_{\text{left}})}$.
- Case 3: The pixel with the lowest measured time is at any other position. In this case the track was neglected for the analysis.

4.1 Drift time

The drift time distributions were accumulated in 15 equally distant interaction depth bins. For each bin the average drift time of the set of prototypical events is calculated. For a model verification, it is shown as function of the interaction depth for different bias voltages and compared to the theoretical predictions (Eq. (5)) in Fig. 6.

Overall, a good agreement of model prediction and measurement was found. An underestimation of the drift times for small z values is discernible, which is possibly due to the inhomogeneity of the electric field, which is stronger for lower z , as the electric field lines are bent towards the pixel electrodes [16].

4.2 z -resolution

The z -resolution was determined by comparing $z_{i, \text{rec.}}$ (calculated according to Eq. (4)) with $z_{i, \text{trajectory}}$.

The evaluation procedure is shown for a single track in Fig. 7.

For a more comprehensive study, the differences $z_{i, \text{trajectory}} - z_{i, \text{rec.}}$ are calculated for every pixel of the preselected prototypical tracks and sorted into 15 depth bins. The

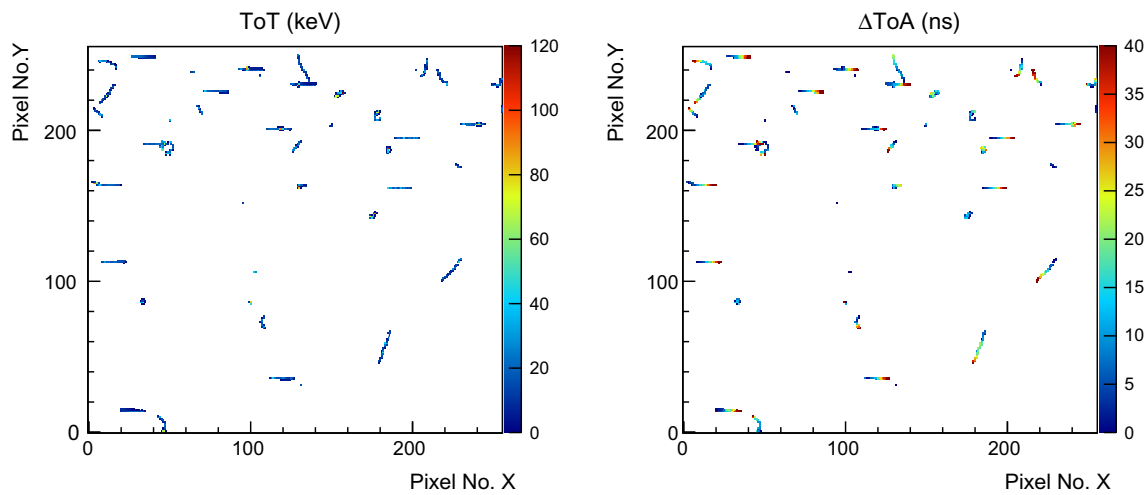


Fig. 5 A set of 50 tracks from the measurement in a 120 GeV/c pion beam. The Timepix3 measures the energy deposit in every pixel (*left*) and the time of the interaction (*right*). The bias voltage was 130 V

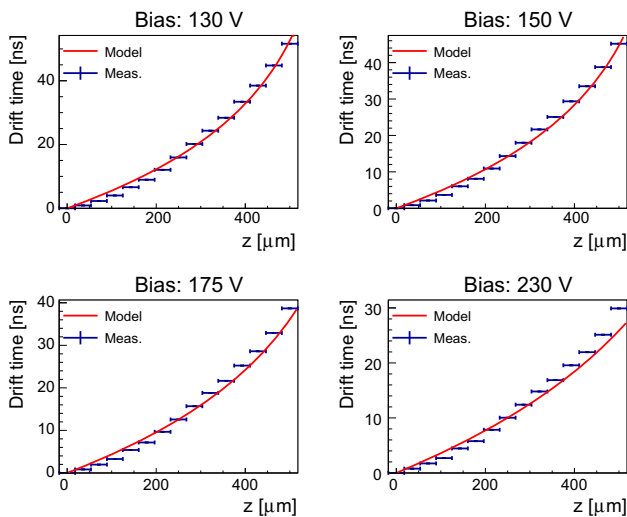


Fig. 6 Comparison of measured and drift times calculated according to Eq. (5) with the parameters given in Table 1 for different bias voltages

Table 1 Overview of silicon sensor related values used for calculating the drift times

Parameter	Description	Value
U_D	Depletion voltage	100 V
μ_h	Mobility of holes	$450 \frac{\text{cm}^2}{\text{Vs}}$ [15]
μ_e	Mobility of electrons	$1350 \frac{\text{cm}^2}{\text{Vs}}$ [15]
d	Thickness of the active sensor	500 μm

resulting distributions are given in Fig. 8. The deviations of the mean values from 0 can be interpreted as the inaccuracy of the drift time model. We thus considered them as the systematic uncertainty Δz_{sys} . The widths σ_z of each distribution describes the dispersion of the measured points around

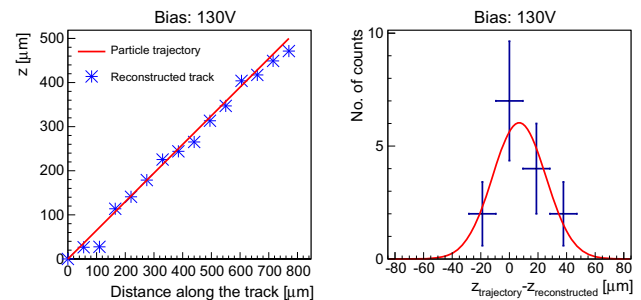


Fig. 7 Comparison of the reconstructed $z_{i,\text{rec}}$ and “real” z -coordinate (obtained from the interpolation of entry and exit point) for a single track. The bias was 130 V

their mean values due to the granularity of the time measurement. We refer to them as the intrinsic uncertainty of the z -determination. It is model independent and remains, even if the drift time could be modeled with absolute accuracy. The total resolution Δz_{total} was estimated conservatively by adding the systematic and intrinsic uncertainties according to

$$\Delta z_{\text{total}} = \sigma_z + \Delta z_{\text{sys}}. \tag{8}$$

Figure 8 shows the above defined resolution and uncertainties as a function of the interaction depth z for the investigated bias voltages. The following observations can be made:

- The best resolution was achieved for the measurement with 130 V bias, where the total z -resolutions are $\leq 50.4 \mu\text{m}$ and the intrinsic z -resolutions are $\leq 28.5 \mu\text{m}$.
- The systematic uncertainties Δz_{sys} are bigger for low z -values and higher bias voltages. To calculate the drift time model, we have assumed a linear electric field throughout the whole sensor depth. This would only be true if the

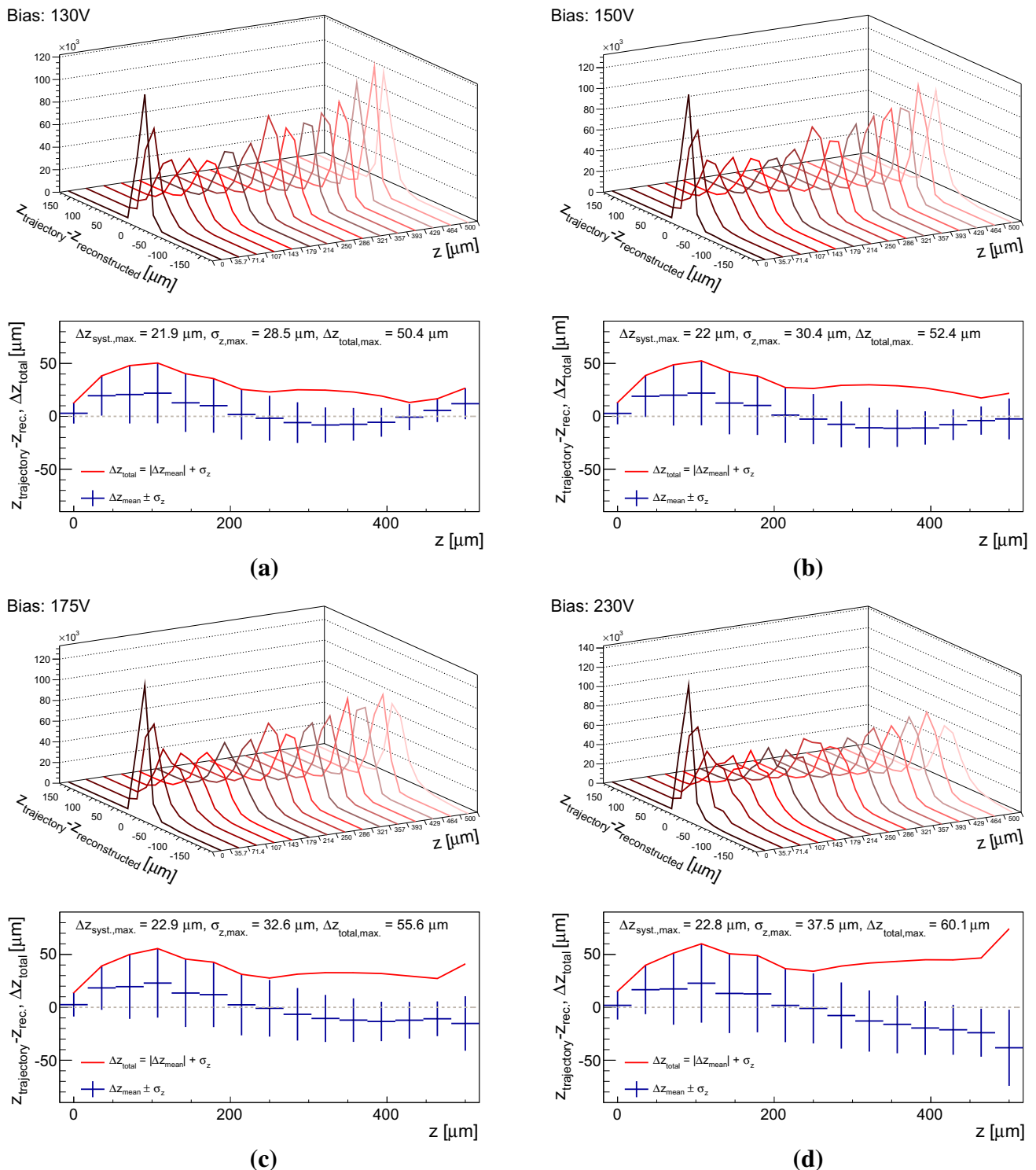


Fig. 8 Depth dependent study of the deviations of the reconstructed from the “real” z -coordinate (*upper plots*) and the z -resolutions as defined in the text (*lower plots*) for the investigated bias voltages: 130 V (a), 150 V (b), 175 V (c), and 230 V (d)

cathode contact was continuous. Since the cathode contact is pixelated, the electric field lines are bent towards the pixel electrodes, thus locally creating a stronger electric field for low z values. For the measurements with

the bias voltages 175 and 230 V, the drift time model additionally underestimates the measurement at high z , indicating that the real electric field is lower than in the linear model.

- The intrinsic resolution σ_z decreases with increasing z and increasing bias. As seen in Fig. 6 the gradient of the drift time curve increases for higher z . Thus, the same drift distances Δz_{drift} yield higher time differences Δt_{drift} at high z than at low z : $\Delta t_{\text{drift}}(z_{\text{high}}) > \Delta t_{\text{drift}}(z_{\text{low}})$ so that the z determination is less prone to inaccuracies arising from the granularity of the time measurement. The same argumentation holds for higher bias voltages, since a higher bias voltage results in smaller drift time differences.

5 Reconstructed particle trajectories

In the following section, tracks are reconstructed regardless of their orientation and size. However, to avoid tracks with an origin inside the sensitive volume (e.g. electrons after gamma ray interactions) and tracks entering at an undefined height from the side, a minimal time difference amongst the cluster pixels' timestamps to allow a full particle penetration through the sensor was required. The input data sets were the measurements at the SPS, and an overnight measurement in the laboratory. The reconstruction outputs are shown for 120 GeV/c pion tracks with long outgoing delta rays in Figs. 9, 10, 11 and 12. Since the pion tracks, fully penetrating the sensor layer, define the reference time frame, the randomly scattered delta electron tracks can be reconstructed three dimensionally.

Figure 13 depicts a straight cosmic muon track from the natural background radiation in Prague (approximately 190m above sea level). The track was fitted by a 3D line (Fig. 13b). As depicted in Fig. 13c the absolute distances from

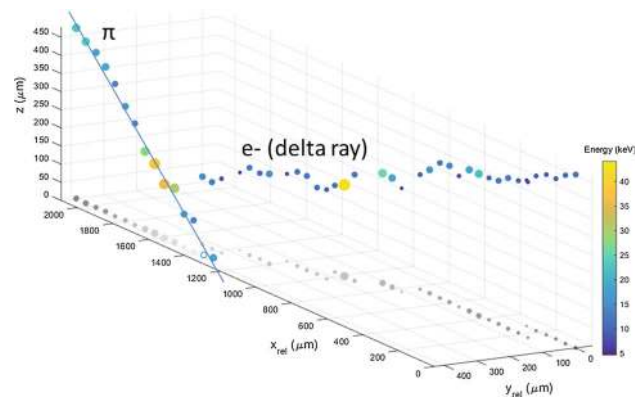


Fig. 9 3D reconstructed 120 GeV/c pion track with outgoing delta ray from the measurement with 130 V bias. The primary pion track passes through the sensitive volume almost undeflected, whereas the secondary electron undergoes multiple scattering along its path. The energy deposition in each pixel is indicated by *color* and corresponds linearly to the radius of the *circles*. The projection in the xy -plane depicts the z -coordinate in *gray scale*. To better illustrate the dimensions of the tracks, the sensitive volume was cropped to the region of interest and relative coordinates were calculated

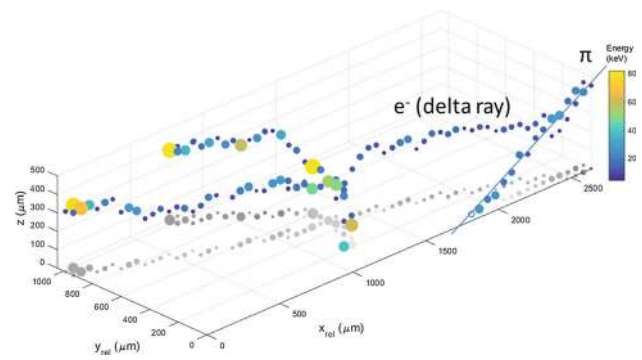


Fig. 10 Same as Fig. 9, but for a track from the measurement with 150 V bias. The secondary particle's track ends in a fork like structure with three prongs

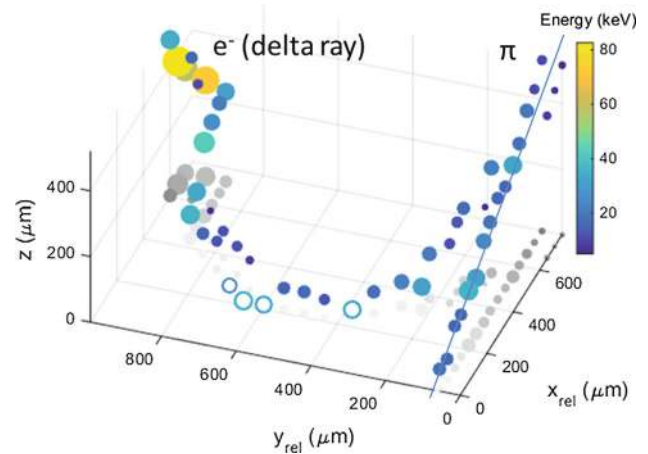


Fig. 11 Same as Fig. 9, but for a track from the measurement with 175 V bias

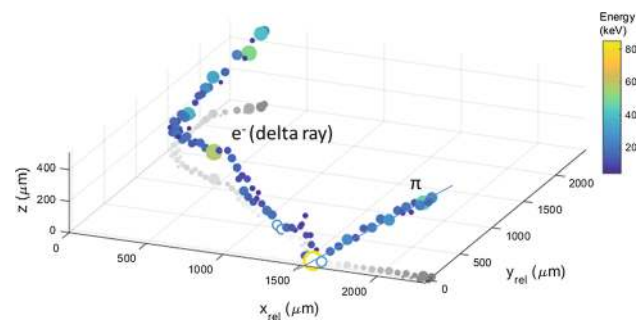


Fig. 12 Same as Fig. 9, but for a track from the measurement with 230 V bias

each reconstructed point to the fit curve can be described by a gaussian distribution with a width of $\sigma_{xyz} = 54.5 \mu\text{m}$, indicating the 3D tracking precision. When sampling the energy losses along the particle trajectory in Fig. 13d, a peak due to a delta ray motion towards either of the contacts is observed. As only 2D projections of each track are measured, the delta ray track is masked by the primary track, so that its trajectory cannot be reconstructed.

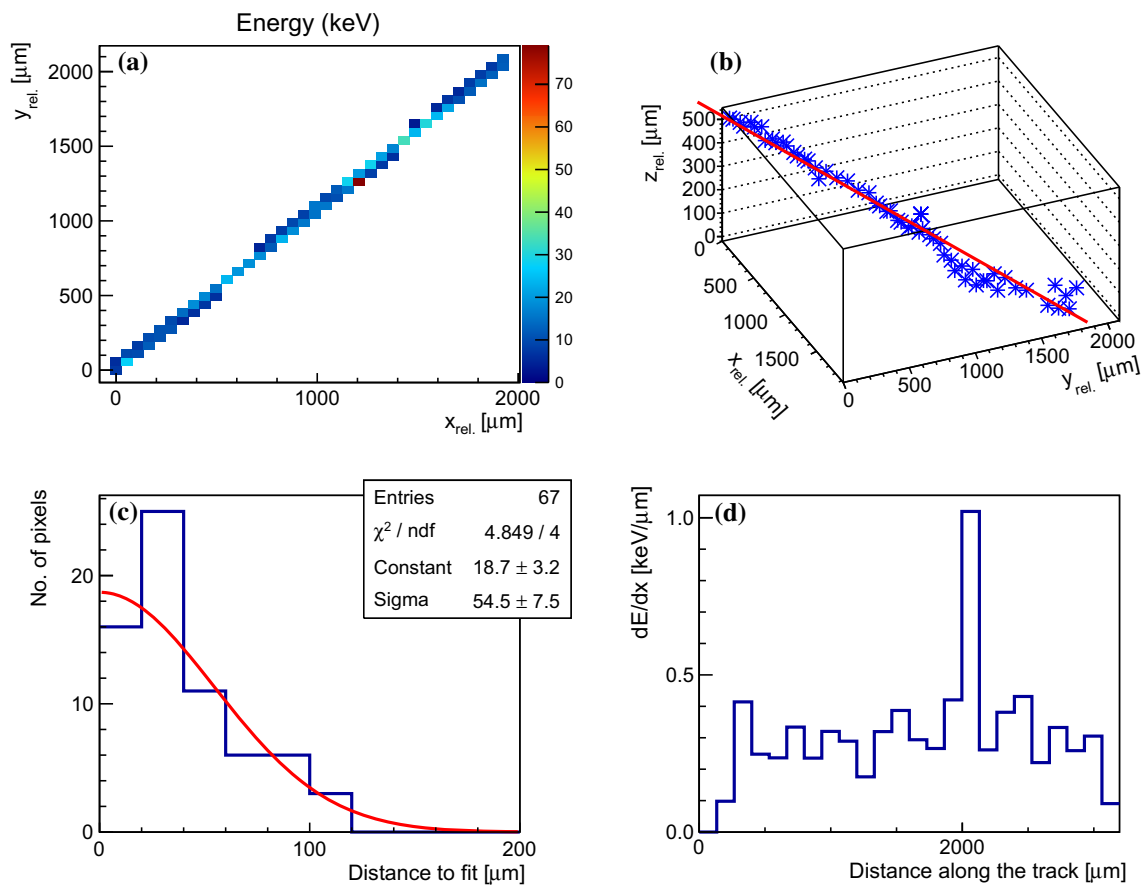


Fig. 13 Cosmic muon track measured in the laboratory. The bias voltage was set to 230 V. **a** The energy projection; **b** a fit to the reconstructed particle trajectory; **c** the distances of each point to the fit; **d** the energy depositions along the track

6 Discussion

The presented work described the application of a hybrid active pixel detector (Timepix3) as a 3D particle tracker, which, by providing information of ionizing energy losses in terms of dissipated energy as well as the time of the interaction, allows a comprehensive analysis of particle tracks. A z -resolution of $50.4 \mu\text{m}$ could be achieved by utilizing the charge carrier drift time information. With an improved description of the drift time dependence on z , the z -resolution could be increased to $28.5 \mu\text{m}$. The presented analysis considered the relative difference of the drift time along a particle trajectory. For this reason an absolute depth-determination can only be provided for particles penetrating the sensor almost completely. However, such events can be extracted reliably by requiring a minimal drift-time difference amongst the pixels of a certain cluster.

A future version of the readout could utilize the electronic signal on the back side contact. The (faster) drift times of the electrons would define a reference time to be used for an absolute determination of the interaction depth. Being challenging due to the high noise level, the feasibility of ana-

lyzing the back-side pulse signal was shown in [17] for a detector of Timepix technology. By this, a fully voxelized 3D volume would be created, also allowing a precise reconstruction of the interaction depths of neutral particles (e.g. neutrons, gamma rays, or photons), particles absorbed in the sensor (or entering from the side), and electrons. This development would be valuable in particular for the experiments measuring the angular correlation functions, the double beta decay rates, and could be exploited for the application of a Timepix3 in a Compton camera.

Acknowledgements The work was done within the Medipix collaboration. We warmly thank the AFP (ATLAS forward physics) team for allowing us a parasitic measurement during their beam time. The work was supported by the Ministry of Education, Youth, and Sports of the Czech Republic under Grant No. LG15052 and the European Space Agency demonstrator Grant with reference TTPM-0006-DOC.

Open Access This article is distributed under the terms of the Creative Commons Attribution 4.0 International License (<http://creativecommons.org/licenses/by/4.0/>), which permits unrestricted use, distribution, and reproduction in any medium, provided you give appropriate credit to the original author(s) and the source, provide a link to the Creative Commons license, and indicate if changes were made. Funded by SCOAP³.

References

1. T. Poikela, J. Plosila, T. Westerlund, M. Campbell, M. D. Gaspari, X. Llopart, V. Gromov, R. Kluit, M. van Beuzekom, F. Zappone, et al., *J. Instrum.* **9**, C05013 (2014). <http://stacks.iop.org/1748-0221/9/i=05/a=C05013>
2. X. Llopart, R. Ballabriga, M. Campbell, L. Tlustos, W. Wong, *Nucl. Instrum. Methods Phys. Res. Sect. A Accel. Spectrom. Detect. Assoc. Equip.* **581**, 485 (2007), ISSN issn0168-9002, notevCI 2007 Proceedings of the 11th International Vienna Conference on Instrumentation. <http://www.sciencedirect.com/science/article/pii/S0168900207017020>
3. J. Jakubek, *J. Instrum.* **4**, P03013 (2009). <http://stacks.iop.org/1748-0221/4/i=03/a=P03013>
4. J. Jakubek, C. Granja, B. Hartmann, O. Jaekel, M. Martisikova, L. Opalka, S. Pospisil, *J. Instrum.* **6**, C12010 (2011). <http://stacks.iop.org/1748-0221/6/i=12/a=C12010>
5. B. Bergmann, T. Michel, A. Surzhykov, S. Fritzsche, *Phys. Rev. C* **94**, 014611 (2016). doi:10.1103/PhysRevC.94.014611
6. C. Granja, S. Polansky, Z. Vykydal, S. Pospisil, A. Owens, Z. Kozacek, K. Mellab, M. Simcak, *Planet. Space Sci.* **125**, 114 (2016). ISSN issn0032-0633. <http://www.sciencedirect.com/science/article/pii/S0032063316300216>
7. S. Gohl, B. Bergmann, C. Granja, A. Owens, M. Pichotka, S. Polansky, S. Pospisil, *J. Instrum.* **11**, C11023 (2016). <http://stacks.iop.org/1748-0221/11/i=11/a=C11023>
8. N. Pacifico, S. Aghion, J. Alozy, C. Amsler, A. Ariga, T. Ariga, G. Bonomi, P. Bräunig, J. Bremer, R. Brusa, et al., *Nucl. Instrum. Methods Phys. Res. Sect. A Accel. Spectrom. Detect. Assoc. Equip.* **831**, 12 (2016), ISSN issn0168-9002, Proceedings of the 10th International 'Hiroshima' Symposium on the Development and Application of Semiconductor Tracking Detectors. <http://www.sciencedirect.com/science/article/pii/S0168900216300808>
9. T. Michel, T. Gleixner, J. Durst, M. Filipenko, S. Geißelsöder, *Adv. High Energy Phys.* **2013** (2013)
10. M. Filipenko, T. Gleixner, G. Anton, T. Michel, *Eur. Phys. J. C* **74**, 3013 (2014), ISSN issn1434-6052. <http://dx.doi.org/10.1140/epjc/s10052-014-3013-1>
11. D. Turecek, J. Jakubek, P. Soukup, *J. Instrum.* **11**, C12065 (2016). <http://stacks.iop.org/1748-0221/11/i=12/a=C12065>
12. J. Jakubek, *Nucl. Instrum. Methods Phys. Res. Sect. A Accel. Spectrom. Detect. Assoc. Equip.* **633**(Supplement 1), S262 (2011), ISSN issn0168-9002, 11th International Workshop on Radiation Imaging Detectors (IWORD). <http://www.sciencedirect.com/science/article/pii/S0168900210013732>
13. D. Nygren, *Proc. PEP Summer Study* (1975)
14. D. Attie, *Nucl. Instrum. Methods Phys. Res. Sect. A Accel. Spectrom. Detect. Assoc. Equip.* **598**, 89 (2009), ISSN issn0168-9002, noteinstrumentation for Colliding Beam Physics Proceedings of the 10th International Conference on Instrumentation for Colliding Beam Physics. <http://www.sciencedirect.com/science/article/pii/S0168900208011996>
15. J. Durst, Ph.D. thesis, Erlangen Center for Astroparticle Physics (2008)
16. B. Kreisler, G. Anton, J. Durst, T. Michel, in *2009 IEEE Nuclear Science Symposium Conference Record (NSS/MIC)* (2009), pp. 1685–1688. ISSN issn1082-3654
17. M. Holik, Ph.D. thesis, University of West Bohemia, Faculty of Electrical Engineering (2015)